Pulse Reformation Algorithm for Leakage of Connected Operators

Gene Stoltz and Inger Fabris-Rotelli

Department of Statistics, University of Pretoria, Pretoria, South Africa

Abstract: The Discrete Pulse Transform (DPT) is a hierarchical decomposition of a signal in *n*-dimensions, built from iteratively applying the LULU operators. The DPT is a fairly new mathematical framework with minimal application and is prone to leakage within the domain, as are most other connected operators. Leakage is the unwanted union of two connected sets and thus provides false connectedness information regarding the data. The Pulse Reformation Framework (PRF) is developed to address the leakage problem within the DPT. It was specifically tested with circular probes and showed successful object extraction of blood cells.

1 INTRODUCTION

The collection of LULU theory and the multiresolution analysis, namely the Discrete Pulse Transform (DPT) was originally developed in (Rohwer, 2005) for one dimension. The LULU operators and the DPT were developed for multi-dimensions (Anguelov and Fabris-Rotelli, 2010).

Within the DPT domain leakage occurs, as for other connected operators. Leakage is the unwanted union of arbitrary sets which heuristically should be separate objects and is further developed theoretically in Section 3. The leakage problem occurs when two disconnected sets, after a certain operation on the space these two sets become either connected as a by-product of the operator, or the sets are connected due to noise, low resolution and other such occurrences.

Leakage is also known as chaining (Soille, 2011). According to (O'Callaghan and Bull, 2005) leakage occurs due to the existence of weak points in the gradient of object boundaries. Leakage is also interpreted as over segmentation. In (Li and Wilson, 1998) the usage of multi-resolution techniques in conjunction with Markov random processes when doing texture segmentation to stop leakage is proposed. A proposed solution to over-segmentation in segmentation with partitioning of connected components based on openings by treating all singletons generated by the operator as elements from larger connected components is discussed in (Ouzounis and Wilkinson, 2005). The larger connected components refer to connectivity classes in higher dimensional space which are extensions of the normally defined connectivity classes in mathematical morphology (Wilkinson, 2005).

Various other attempts has been made for creating solutions to the leakage problem, including redefining existing connectivities (Goutsias et al., 2000), (Tzafestas and Maragos, 2002), (Wilkinson, 2008)(Goutsias et al., 2000)(Tzafestas and Maragos, 2002) (Wilkinson, 2008). Another attempt at reducing leakage is the definition of stopping criteria in morphological opening and opening by reconstruction (Terol-Villalobos et al., 2006). Serra also suggested the idea of using a circular structuring element to refine connectivity in order to deal with leakage (Serra, 2005).Leakage exists in other image processing spaces such as the active-contour model where possible reduction in leakage is to estimate the position of possible edges in the image by minimal weighted local variance (Law and Chung, 2006). Graham et al (Graham et al., 2008) used adaptive parameters within the active-contour model to possibly stop estimated leakage.

We propose a framework called Pulse Reformation Framework (PRF) to resolve leakage within the DPT domain. The framework is developed for two dimensional data which includes any type of image in the conventional sense. We use circular probes to resolve leakage in the domain, however alternatives are easily interchangeable. The framework is applied to a small set of blood cells. On basis of the PRF within the LULU scale-space a spot detector is developed and compared.

2 THE DISCRETE PULSE TRANSFORM

An n-monotone sequence is part of a connectivity class and is thus a connected set. The concept of an n-monotone sequence is extended to higher dimensions with the introduction of connectivity classes (Serra, 1982).

Definition 2.1. Let E be an arbitrary nonempty set. A family $C \in \mathcal{P}(E)$ is called a connectivity class if the following axioms hold: (1.) $\emptyset \in C$ (2.) $\{x_i\} \in C$ for every i such that $x_i \in E$ (3.) For each $C_j \in C$ and $\bigcap_{j \in I} C_j \neq \emptyset$, then $\bigcup_{j \in I} C_i \in C$.

Any element of C is called a connected set. We can now extend to d-dimensions such that $x \in \mathbb{Z}^d, d \in \mathbb{N}$ so that the LULU operators operate on n-connected sets in d-dimensions but with a discrete space is sufficiently rich in connected sets. The required conditions for such a rich connectivity space is found in (Anguelov and Fabris-Rotelli, 2010).

For any set of cardinality $n + 1$ we can now define within the d-dimensional space connected sets which contain the point $x \in \mathbb{Z}^d$, $\mathcal{N}_n(x) = \{V \in C : x \in V, \mathtt{card}(V) = n+1\}$. The LULU operators defined on an Abelian group $\mathcal{A}(\mathbb{Z}^d)$ such that commutativity always holds within the lattice, are as follows:

Definition 2.2. Let $f \in \mathcal{A}(\mathbb{Z}^d)$ and $n \in \mathbb{N}$. Then for $x \in \mathbb{Z}^d$: $L_n(f)(x) = \max_{V \in \mathcal{N}_n(x)} \min_{y \in V} f(y)$ and $U_n(f)(x) = \min_{V \in \mathcal{N}_n(x)} \max_{y \in V} f(y)$.

The operators defined in Definition 2.2 operate only on local maximum sets and minimum sets in the space. With the concept of adjacency we can classify a connected set as a local minimum or a local maximum.

Definition 2.3. Let $V \in C$ and $f \in \mathcal{A}(\mathbb{Z}^d)$ then V is called a local maximum (minimum) set if:

$$\mathtt{max(min)}_{y \in \mathtt{adj}(V)}\{f(y)\} < (>)\mathtt{min(max)}_{x \in V}\{f(x)\},$$

where $\mathtt{adj}(V) = \{x \in \mathbb{Z}^d : x \notin V, V \cup \{x\} \in C\}$.

The L_n operator removes local maximums of size smaller and equal to n while U_n removes local minimums of size smaller or equal to n. The two operators can't create new local maximum sets or minimum sets but they may enlarge the cardinality of a connected set attributed to it. The LULU operators maintain their properties from the one dimensional theory such as being a separator, being fully trend preserving and preserving total variation, as well as all other properties. The DPT in multi-dimensions is represented as $DPT(f) = [D_1(f), D_2(f), ..., D_{N-1}(f)]$. Each component D_n is calculated as

$$D_1(f) = (I - P_1)(f)$$

$$D_n(f) = (I - P_n) \circ Q_{n-1}(f), \ \ n = 2, ..., N-1$$

where $P_n = L_n \circ U_n$ or $P_n = U_n \circ L_n$ and $Q_n = P_n \circ ... \circ P_1, n \in \mathbb{N}$.

Definition 2.4. A function $\psi \in \mathcal{A}(\mathbb{Z}^d)$ is called a pulse if there exists a connected set V and a nonzero real number α such that

$$\psi(x) = \begin{cases} \alpha, & if \ x \in V \\ 0, & if \ x \in \mathbb{Z}^d \backslash V. \end{cases}$$

Each different scale D_n is then $D_n(f) = \sum_{s=1}^{\gamma(n)} \psi_{ns}$ and

$$f = \sum_{n=1}^{N-1} \sum_{s=1}^{\gamma(n)} \psi_{ns}$$

where $\gamma(n)$ is the total number of local maximum and local minima of size n and ψ is a pulse (def 2.4).

The DPT decomposition forms a scale-space formally defined in: (Fabris-Rotelli, 2012):

Definition 2.5. Let $f \in \mathcal{A}(\mathbb{Z}^d)$. The set $\mathcal{S}_{f,\Lambda} = \{(\lambda, \mathcal{L}_f(\lambda)) : \lambda \in \Lambda\}$ is called a scale-space of f generated by the operator $\mathcal{L}$ with respect to scale parameter set Λ and measure of smoothness $S \in \mathcal{A}(\mathbb{Z}^d)$.

S is a function called the measure of smoothness which is dependant on the requirement of the specific task. Overall a very smooth signal yields a smoothness measure of 0 where rougher signals yield higher values. In the case of the DPT the measure of smoothness determines how close the current sequence is to its local monotonicity (Fabris-Rotelli, 2012). The interested reader can find more information in *Discrete Pulse Transform of images and applications* (Fabris-Rotelli, 2012). Some relations with mathematical morphology are however obvious. Firstly the LULU smoothers are exactly the area opening and closing operators (Vincent, 1193), but were developed independently from the one-dimensional LULU smoothers (Rohwer, 2005; Rohwer and Laurie, 2006; Rohwer and Toerien, 1991). They can thus be compared to a morphological pyramid (Salembier and Serra, 1995; Morales et al., 1995), but are however valid in N dimensions and do not require the restriction of a predetermined structuring element. The DPT does replicate the nice property of a morphological pyramid of nested flat zones, allowing for image simplification while preserving contour information.

The DPT forms the scale-space $\mathcal{S}_{f,LULU} = \{(n, P_n(f)) : n \in \Lambda_0 = \{0, 1, 2, ..., N\}\}$ called the LULU scale-space. A scale-space allows the tracking of structures within a domain through different scales ranging from fine to coarse.

3 LEAKAGE

We provide a formal definition for leakage as:

Definition 3.1. Let $\Phi : \mathbb{Z}^d \to \mathbb{Z}^d$ be an arbitrary operator. If there exists $\{X_i \subset \mathbb{Z}^d, i \in I, X_i \in \mathcal{C}\}$ with $\cap_{i \in I} X_i = \emptyset$ such that $\cup_{i \in I} \Phi(X_i) \in \mathcal{C}$ then Φ is said to have caused leakage.

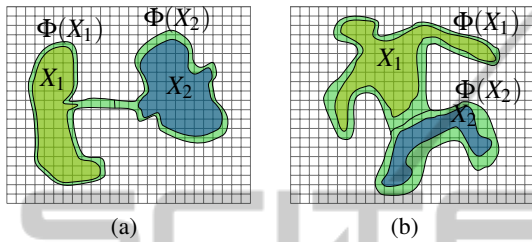An operator Φ may satisfy Definition 3.1 in different mannerisms. Consider Figure 1, an example of desired and undesired leakage.

Figure 1: (a) Undesired Leakage, (b) Desired leakage.

In Figure 1(a), after applying operator Φ, the leakage formed is undesired. Object $\Phi(X_1)$ and $\Phi(X_2)$ should be separate objects. However, in Figure 1(b) object X_1 and X_2 should be one. After applying the operator to the image the two objects get connected as desired. Leakage are generally dealt with by directly applying a problem specific solution. TO distinguish between different kinds of leakage we define a measure of observed leakage as follows:

Definition 3.2. The strength of a leakage is measured as $1/\text{card}(A_{Strength})$ where $A_{Strength} = \{\{x_i, x_j\} \in \mathcal{C} : x_i \in \Phi(X_i), x_j \in \Phi(X_j), i \neq j, i, j \in I\}$.
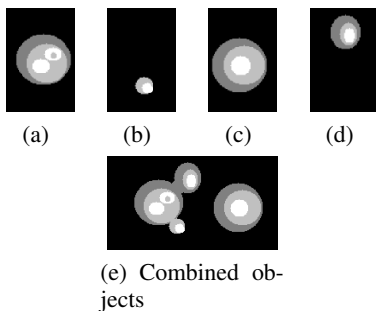

(e) Combined objects

Figure 2: Synthetic Objects in an image.

The larger the strength of the leakage the larger the undesired effect is on the image. It is clear then in the case of a good smoother desired leakage will occur.

A synthetic example is created to demonstrate the leakage problem. Four objects with varying internal intensities shown in Figure 2 are combine into a single image. The four objects need to be extracted.

To extract the different objects we can use connected components to indicate individual objects. A set consisting of connected components will then denote one object. Two simplistic methods can be used. The first is the use of thresholding. The synthetic image can be thresholded at three different levels as the image only consists of four discrete grey levels. The thresholded images are shown in Figure 3. In Figure 3 it is clear that no threshold will yield 4 connected sets which will cohere with the four original objects. Another way, is to use the DPT scale-space and threshold different pulse sizes. We choose four different pulse ranges which are shown in Figure 4.
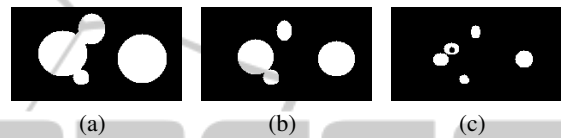

Figure 3: Synthetic image thresholded at 3 different levels.

(a) $n \in [0, 400)$ (b) $n \in [400, 3600)$

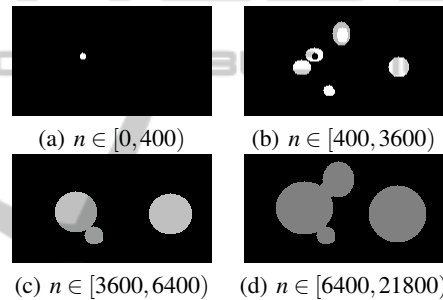(c) $n \in [3600, 6400)$ (d) $n \in [6400, 21800)$

Figure 4: Synthetic images thresholded for different pulse ranges.

Even using the DPT scale-space it is not possible to extract four connected components that will yield the required connected sets. In Figure 3 and 4 leakage is evident in most of the thresholded images. Although technically there exist many other ways to possibly extract the objects, this problem was only used to illustrate leakage in simple connected components and DPT framework. In the next section we describe a proposed method to eliminate leakage within the DPT framework.

4 THE PULSE REFORMATION FRAMEWORK (PRF)

To explain the proposed framework one can visualize the leakage problem as a box of brittle magnets. The task is to successfully remove all the magnets from the box and place the individual ones in a row. The problem lies in identifying these individual magnets. Two or more magnets can be stuck together and

must be pulled apart. However an individual magnet can only be separated from itself by breaking it. By looking at structural cues we can separate these magnets, such as if two balls are stuck together they most probably must be separated. If two cubes, unaligned, are stuck together we can assume they must be separate. If a sphere and a pyramid are stuck together they must probably be separated. We can thus continue like this for all kinds of known shapes and say with high probability that these different structures do not fit together.
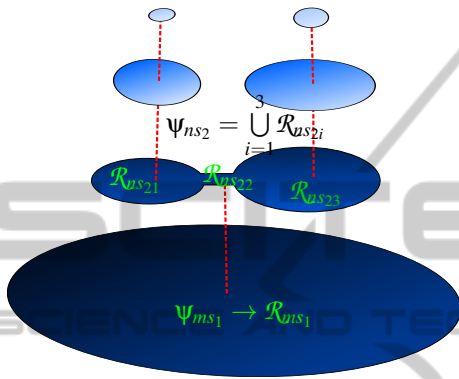

Figure 5: A DPT pulses stacked in different scale.

The scales from the DPT can be stacked from the smallest to the largest scale forming the LULU scale-space. A visual demonstration is shown in Figure 5. The pulses in Figure 5 are said to form a stack defined by the scale-space neighbourhood relation given below in Definition 4.1 and Definition 4.2.

Definition 4.1. Two arbitrary DPT pulses, ψ_{ns_2} and ψ_{ms_1} with $n < m$, are called scale-space neighbours if $\psi_{ns_2} \subset \psi_{ms_1}$ and for any other DPT pulse ψ_{ps_3}, $n < p < m$ we have $\psi_{ps_3} \cap \psi_{ns_2} = \emptyset$.

The strength of the scale-space neighbour relation is measured as the inverse of the difference in cardinality of the two pulses ϕ_{ns_2} and ϕ_{ms_1}, naturally $\frac{1}{m-n}$.

Definition 4.2. A collection of DPT pulses are said to form a stack if they are each scale-space neighbours of at least one other pulse in the collection.

In Figure 5 the pulses illustrated form a stack. The PRF algorithm will obtain the true pulses $\mathcal{R}_{us_{21}}$, $\mathcal{R}_{us_{22}}$ and $\mathcal{R}_{us_{23}}$.

By using Definition 4.2 we can say that every pulse consists of regions so that $\psi_{ns} = \bigcup_{i=1}^{p} \mathcal{R}_{us_k}$. This is demonstrated in Figure 6. Assume that Figure 6 is an image of two separate balls, thus two individual objects. Inspecting Figure 6, only one object is observed, the full pulse ψ_{ns_2}. The two objects are linked by a third region. The third object is then referred to

as a leakage region, which on its own can possibly also be an object or noise. If we want to eliminate leakage we need to estimate the true regions $\mathcal{R}_{us_{21}}$, $\mathcal{R}_{us_{22}}$ and $\mathcal{R}_{us_{23}}$.
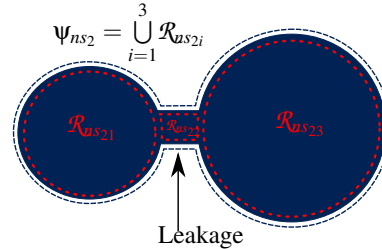

Figure 6: A pulse extracted by the DPT showing the possible regions which the pulse consists of.

We aim to, in the LULU scale-space, objectively eliminate leakage. In case of the magnet box we aim at finding all the rigid shapes with the most probable shape having the least amount of edges. We can then objectively eliminate leakage.

The proposed framework will be developed using circular probes. Other shapes can also be used within the framework. Using the PRF, circular object within the LULU scale-space will produce strong joined stacks. A *joined stack* is formed when a group of scale-space neighbours forming a stack also cohere to an additional requirement. The additional requirement involves a *principle point* $\tilde{\mathcal{R}}_{us_k}$ for each region $\mathcal{R}_{us_k}$. The principle point needs to capture the core structure of the region. The principle point of circular object is at the arithmetic mean in terms of the spatial domain, is always surrounded by edges and the point lies within the object. It can be assumed that the centre of a circle will capture the core purpose of circular objects. The circular object can also be reconstructed from the principle point by iteratively increasing the radius of the circle centred at the principle point. In general if using any shaped probe, the principle point $\tilde{\mathcal{R}}_{us_k}$ should be scale invariant, translation invariant, rotation invariant, and affine invariant.

In Figure 7 the red dot shows the principle point and the dark blue shows elements part of the geometrical set. The principle point of the doughnut shape in Figure 7 can be defined as the centre of a circle which is not contained within the set but is surrounded by a continuous edge. The principle point of a concave mirror shape should lie at the focal point of the concave side of the set. The principle point of a triangle should lie in the middle of the shortest edge. From all of these principle points the objects can be reconstructed by knowing one extra parameter such as the radius or distance of a corner or edge in the set. To estimate a region's principle point, we iteratively erode the pulse until the next erosion yields an empty set.

Figure 8 illustrates this. The last non-empty erosions will represent the principle points of the regions and also indicated the number of regions the pulse is made up of. The regions can then be reconstructed by dilating each principle point until the defined energy function E_{ns} below is minimized over every region of the pulse simultaneously.

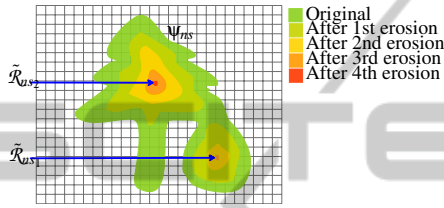Figure 7: Examples of possible principle points denoted by the red dot.

Figure 8: Example of finding the principle points in a pulse.

Each region $\mathcal{R}_{as_k}$ will have a principle point, thus each pulse can contain multiple principle points. The regions must adhere to the boundary conditions of the DPT scale-space thus

$$\mathcal{R}_{as_k} = \left(\mathcal{R}_{as_k} \cap \psi_{ns} \right) / \bigcup_{k \neq i} (\mathcal{R}_{as_i}). \tag{1}$$

The regions within a pulse can only consist of unique elements thus every element in a pulse can only be assigned to one region. From the principle point each region is reconstructed by minimizing the energy function E_{ns}. For the circular probes we can define an energy function

$$E_{ns} = \sum_{k=1}^{p} \sum_{t=1}^{\kappa(s_k)} \frac{\mathtt{card}\{\zeta(t-1, \tilde{\mathcal{R}}_{as_k})\}}{|\mathtt{card}\{\zeta(t, \tilde{\mathcal{R}}_{as_k})\} - \mathtt{card}\{\zeta(t-1, \tilde{\mathcal{R}}_{as_k})\}|}$$

where $\zeta(t, \tilde{\mathcal{R}}_{as_k})$ denotes a set containing all the elements within a circle of radius t centred at $\tilde{\mathcal{R}}_{as_k}$, the tth dilation of the circular set centred at the principle point, while staying within the boundary of the pulse; where p is the number of regions; and $\kappa(s_k)$ the appropriate t number of dilations where t is a geometrical parameter. The energy function determines the best circles centred at the principle points associating each pulse element to a region, restricted to the boundary conditions in equation 1. The created regions and found principle point can be compared techniques such as the medial axis transform and the resulting skeleton by maximal balls (LVincent and Dougherty, 1994).

Next we need to relate regions at different scales to one another. Each region has the apparent same defining principle point which should then be positioned at a known position between scales. Specifically for circular objects all the principle points should be at the same geometrical position. We can thus say that two or more regions form a joined stack (Definition 4.4) if the principle point(s) are joined (Definition 4.3) and the regions form a stack (Definition 4.2).

Definition 4.3. Two scale-space neighbours ψ_{ns} and ψ_{ms} with $n < m$ containing regions $\mathcal{R}_{as_j}$ and $\mathcal{R}_{ms_i}$ with geometrical parameters r_j, r_i and principle points $\tilde{\mathcal{R}}_{as_j}$, $\tilde{\mathcal{R}}_{ms_i}$, are said to have joined principle points if $J(\tilde{\mathcal{R}}_{as_j}, \tilde{\mathcal{R}}_{ms_i}) < \varepsilon = \mathcal{N}(\tilde{\mathcal{R}}_{as_j}, \tilde{\mathcal{R}}_{ms_i}, r_i, r_j)$ where J is the joining function and $\mathcal{N}$ is a noise function.

The joining function J provides a relation between of the two principle points and can be any type of polygon or line. The noise function $\mathcal{N}$ provides a measure of how similar the two regions are based on the expected relative position of the principle points. For the circular case we define $r_j = \kappa(s_j)$, $r_i = \kappa(s_i)$ and $J(\tilde{\mathcal{R}}_{as_j}, \tilde{\mathcal{R}}_{ms_i}) = \|\tilde{\mathcal{R}}_{as_j}, \tilde{\mathcal{R}}_{ms_i}\|$ with $\|\cdot, \cdot\|$ giving the euclidean distance between the two points. We also define our noise function $\mathcal{N}(\tilde{\mathcal{R}}_{as_j}, \tilde{\mathcal{R}}_{ms_i}, \kappa(s_i), \kappa(s_j))$ $= (\mathtt{card}\{\mathcal{R}_{ms_i}\}/\mathtt{card}\{\mathcal{R}_{as_j}\}) * (\kappa(s_i)/\kappa(s_j))$.

Definition 4.4. Two regions $\mathcal{R}_{as_j}$ and $\mathcal{R}_{ms_i}$ with $n < m$ form a joined stack if their principle points are joined and $\mathcal{R}_{as_j} \subseteq \mathcal{R}_{ms_i}$.

This definition is visually shown in Figure 9 where $J(\tilde{\mathcal{R}}_{as_j}, \tilde{\mathcal{R}}_{ms_i}) = a$. The ε can be interpreted as a noise canceller within the LULU scale-space. If a perfect scale-space was constructed all the pulses forming joinings belong to the same object and will have aligned principle points. In Figure 9 the large coloured dots denote the principle point in each region.
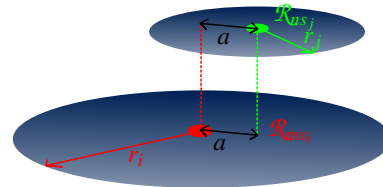

Figure 9: The joining of two arbitrary pulses.

The strength of the joining of the two regions can be measured as the strength of a scale-space neighbour. The smaller the difference in cardinality of the two regions, the stronger the joining becomes. An additional strength measure can be added such as the variation of the principle points from the expected distance.

We have now shown that we can estimate regions from pulses. We estimate a region from the first estimated principle point and then re-estimate the principle point using the region. This process can be repeated until the principle point moves less than the noise function $\mathcal{N}$ and E_{ns} is minimized.

The estimation of the regions within pulses can be represented by a four corner model. The four nodes are the *Principle Point* node, the *Pulse* node, the *Joining* node and the *Regions* node. The nodes are shown in Figure 10(a). Each node's name is self-evident of the represented data at the node. The arrows present the process that needs to be executed to transform one set of data to another.
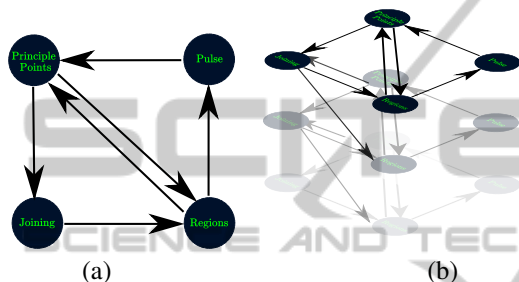

(a)　　　　　(b)

Figure 10: (a) Region based Pulse Reformation Model. (b) Region based Pulse Reformation Model.

The *Pulse* node can be used to estimate the *Principle Points* node. The *Principle Points* node is used to estimate the *Regions* and to determine joining with other scale-space neighbour regions. The *Joining* node can be used to estimate the *Regions* node. The *Regions* node can estimate the *Principle Points* as well as the *Pulse* node. This whole process follows an iterative nature.

To create a more robust estimation of the regions we need to estimate each region by including the structure of the complete LULU scale-space. The PRF uses an iterative approach to first estimate an initial principle point which is used to estimate the regions within each pulse. The principle points that form a joined stack can be used to adjust principle points and re-estimate the regions until all energy functions E_{ns} and all joining functions $J(\cdot)$ have been minimized. This combined iterative model is represented in Figure 10(b).

After the PRF has been applied the LULU scale-space consists of various joined stacks. Each joined stack will have a *joined stack strength* which is calculated by the sum of the strength of the scale-space neighbours within the joined stack divided by the number of regions contained in the joined stack. The strongest joined stacks will then present the most salient objects.

To be able to use the PRF four main things need

to be defined: (1.) The Principle Point Estimator $\tilde{\mathcal{R}}_{as_k}$. (2.) The Energy function E_{ns} which needs to be minimized. (3.) The joining function $J(\cdot)$. (4.) The noise function or principle point alignment ε. Each of these functions have already been defined for the case of circular objects.

5 SYNTHETIC LEAKAGE REDUCTION

We can now apply the PRF to the synthetic image created in Figure 2. In Figure 11 the output of the framework is shown. Four different objects were extracted each coinciding with a synthetic object. Each extracted object shows protrusion where leakage occurred. This is where the framework has an uncertainty as to which principle point the region elements belong.
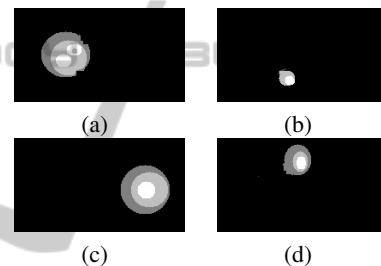

(a)　　　　　(b)

(c)　　　　　(d)

Figure 11: The Pulse Reformation of the synthetic image.

The extracted objects can easily be thresholded just above zero to provide four discrete connected sets which then coincide with the original objects. The PRF can now be tested on a real world image. Another example application appears in (Fabris-Rotelli and Stoltz, 2012).

6 SPOT DETECTION

The PRF can be used for spot detection. We can not only extract the strongest joined stacks but only the joined stack who's bottom region or top region is within a certain range. For spot detection the bottom region of the joined stack must be smaller or equal to the largest expected spot.

Fixed cell imaging of individual mRNA molecules is accomplished by using 48 or more singly labelled oligonucleotide probes (Raj et al., 2008). By utilizing fluorescent microscopy the mRNA becomes computationally identifiable fluorescent spots. There can be hundreds of mRNA in a cell. An effective spot detector and spot counter is thus required.

A current spot detector exists which uses thresholding of a difference of two Gaussians (Raj et al., 2008). The DoG spot detector has three different parameters which can be modified: the range of the Gaussian window, the variance of the Gaussian and the specific threshold. In depth the method actually has 5 parameters as both the Gaussians must be selected, each with a window and a variance. Usually one Gaussian is assumed to be the original image.

Our spot detector will only use the joined stacks with a bottom pulse cardinality smaller than a set size. These joined stacks are then thresholded by the joined stack strength to remove the very weak joined stacks. The PRF spot detector then only uses 2 parameters: the expected size of the objects and the threshold value.

For the experiment we created our own ground truth. The ground truth was not evaluated by an expert in mRNA thus we can not measure the algorithms true performance but only the relative performance. The DoG spot detector was confirmed to be an accurate detector but was not quantified (Raj et al., 2008). The two test images and their ground truths are shown in Figure 12.

(a)   (b)

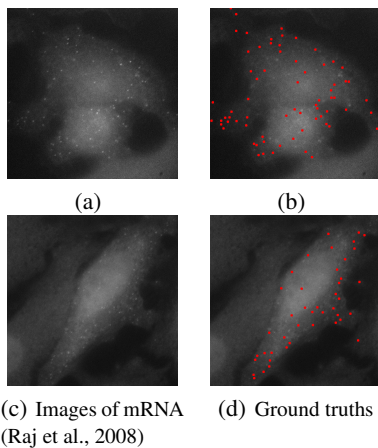(c) Images of mRNA   (d) Ground truths
(Raj et al., 2008)

Figure 12: Fluorescent microscopy images of mRNA.

The two algorithms will be evaluated by using precision-recall graphs (Powers, 2011). The precision ($tp/(tp + fp)$) and recall ($tp/(tp + fn)$) is used to calculate the f-measure:

$$F\text{-measure} = 2 \cdot \frac{\text{Precision} \cdot \text{Recall}}{\text{Precision} + \text{Recall}}.$$

The true positives, tp, are measured by taking the number of correctly detected spots thus the detected spots that coincide with the ground truth. The false positives, fp, are measured by all the spots that do not coincide with ground truth. If two spots are detected close together and both coincide with one spot on the ground truth, one is taken as correct and the other is then a false positive. The false negatives, fn, are calculated as all the spots in the ground truth that were not detected by the spot detection algorithm.
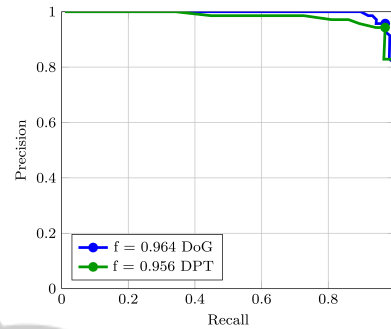

Figure 13: The first Precision-Recall graph for the DPT and DoG spot detectors.
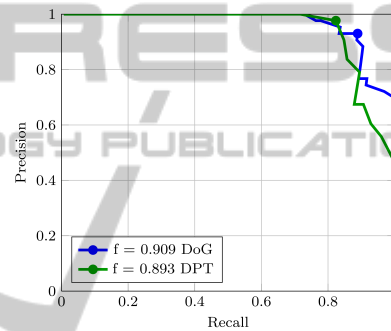

Figure 14: The second Precision-Recall graph for the DPT and DoG spot detectors.

In Figures 13 and 14 the f-measures are plotted for increasing threshold values. The maximum f-measures are indicated on the graphs.

Both the algorithms perform well. The PRF spot detector using the DPT is 1% less accurate than the DoG method. Taking into account that the DPT method has 3 less parameters to tune than the DoG method and is less sensitive to its parameters the DPT method is superior to the DoG method. The sensitivity of the DoG method to the chosen variance parameter is high as the chosen variance propagates to each pixel in the image. Choosing the correct variance for a Gaussian function is also not a trivial matter. The DPT method is not very sensitive to the expected size of the spot as long as the expected size is greater than the actual size of the spot. The expected size of the spot is easily measured by looking at the number of pixels within the spot.

7 CONCLUSION

We have provided a theoretical settings for leakage

within the DPT as well as an effective algorithm to deal with leakage in images and have applied the technique to salient object detection and a more specific application in spot detection within the DPT framework. Future work will look at developing a non-shape dependent reformation algorithm taking advantage of the non-shape dependent nature of the DPT. In addition, relaxing the pulse definition to allow for quasi-flat connected components (Soille, 2011) may add to a more efficient DPT as well as a more robust reformation algorithm.

ACKNOWLEDGEMENTS

REFERENCES

Anguelov, R. and Fabris-Rotelli, I. (2010). LULU operators and Discrete Pulse Transform for multidimensional arrays. *Image Processing, IEEE Transactions on*, 19(11):3012–3023.

Fabris-Rotelli, I. and Stoltz, G. (2012). On the leakage problem with the Discrete Pulse Transform decomposition. In de Waal, A., editor, *Proceedings of the 23rd Annual Symposium of the Pattern Recognition Association of South Africa*, pages 179–186.

Fabris-Rotelli, I. N. (2012). *Discrete Pulse Transform of images and applications*. PhD thesis, University of Pretoria.

Goutsias, J., Vincent, L., and Bloomberg, D. S. (2000). *Mathematical morphology and its applications to image and signal processing*, volume 18, chapter Practical extensions of connected operators, pages 97–110. Springer.

Graham, M. W., Gibbs, J. D., and Higgins, W. E. (2008). Robust system for human airway-tree segmentation. In *Medical Imaging*, pages 69141J–69141J. International Society for Optics and Photonics.

Law, W. and Chung, A. C. (2006). Minimal weighted local variance as edge detector for active contour models. In *Computer Vision–ACCV 2006*, pages 622–632. Springer.

Li, C.-T. and Wilson, R. (1998). Image segmentation based on a multiresolution bayesian framework. In *Image Processing, 1998. ICIP 98. Proceedings. 1998 International Conference on*, pages 761–765. IEEE.

LVincent and Dougherty, E. (1994). *Digital Image Processing Methods*, chapter Morphological segmentaion fro textures and particles, page Chapter 2. Marcel Dekker, Inc.

Morales, A., Acharya, R., and Ko, A.-J. (1995). Morphological pyramids with alternating sequential filters. *IEEE Transactions on Image Processing*, 4(7):965–977.

O'Callaghan, R. J. and Bull, D. R. (2005). Combined morphological-spectral unsupervised image segmentation. *Image Processing, IEEE Transactions on*, 14(1):49–62.

Ouzounis, G. K. and Wilkinson, M. H. (2005). Countering oversegmentation in partitioning-based connectivities. In *Image Processing, 2005. ICIP 2005. IEEE International Conference on*, volume 3, pages III–844. IEEE.

Powers, D. M. (2011). Evaluation: from precision, recall and f-measure to roc, informedness, markedness & correlation. *Journal of Machine Learning Technologies*, 2(1):37–63.

Raj, A., van den Bogaard, P., Rifkin, S. A., van Oudenaarden, A., and Tyagi, S. (2008). Imaging individual mrna molecules using multiple singly labeled probes. *Nature methods*, 5(10):877–879.

Rohwer, C. (2005). *Nonlinear Smoothers and Multiresolution Analysis*. Birkhauser.

Rohwer, C. and Laurie, D. (2006). The Discrete Pulse Transform. *SIAM journal on mathematical analysis*, 38(3):1012–1034.

Rohwer, C. and Toerien, L. (1991). Locally monotone robust approximation of sequences. *Journal of computational and applied mathematics*, 36(3):399–408.

Salembier, P. and Serra, J. (1995). Flat zones filtering, connected operators, and filters by reconstruction. *IEEE Transactions on Im*, 4(8):1153 – 1160.

Serra, J. (1982). *Image Analysis and Mathematical Morphology. Vol I, and Image Analysis and Mathematical Morphology. Vol II: Theoretical Advances*. Academic Press, London.

Serra, J. (2005). Viscous lattices. *Journal of Mathematical Imagin*, 22:269–282.

Soille, P. (2011). Preventing chaining through transitions while favouring it within homogeneous regions. In Soille, P., Pesaresi, M., and Ouzounis, G., editors, *Mathematical Morphology and Its Applications to Image and Signal Processing*, volume 6671 of *Lecture Notes in Computer Science*, pages 96–107. Springer Berlin Heidelberg.

Terol-Villalobos, I. R., Mendiola-Santibáñez, J. D., and Canchola-Magdaleno, S. L. (2006). Image segmentation and filtering based on transformations with reconstruction criteria. *Journal of Visual Communication and Image Representation*, 17(1):107–130.

Tzafestas, C. S. and Maragos, P. (2002). Shape connectivity: multiscale analysis and application to generalized granulometries. *Journal of Mathematical Imaging and Vision*, 17(2):109–129.

Vincent, L. (1193). Grayscale area opening and closings, their efficient implementation and applications. In *Proceedings of the EURASIP Workshop on Mathematical Morphology and its Applications to Signal Processing*, Barcelona, Spain.

Wilkinson, M. (2005). Attribute-space connected filters. In Ronse, C., Najman, L., and Decencire, E., editors, *Mathematical Morphology: 40 Years On*, volume 30 of *Computational Imaging and Vision*, pages 85–94. Springer Netherlands.

Wilkinson, M. H. (2008). Connected filtering by reconstruction: Basis and new advances. In *Image Processing, 2008. ICIP 2008. 15th IEEE International Conference on*, pages 2180–2183. IEEE.